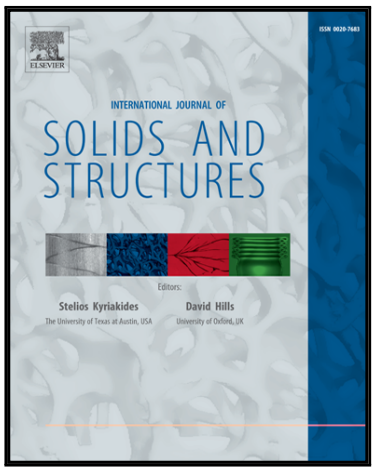

Snell's law of elastic waves propagation on moving property interface of time-varying materials

Langquan Shui , Yilun Liu , Xi Chen

PII: S0020-7683(18)30062-3
DOI: 10.1016/j.ijsolstr.2018.02.013
Reference: SAS 9901

To appear in: *International Journal of Solids and Structures*

Received date: 6 June 2017
Revised date: 23 December 2017
Accepted date: 10 February 2018

Please cite this article as: Langquan Shui , Yilun Liu , Xi Chen , Snell's law of elastic waves propagation on moving property interface of time-varying materials, *International Journal of Solids and Structures* (2018), doi: 10.1016/j.ijsolstr.2018.02.013

Snell's law of elastic waves propagation on moving property interface of time-varying materials

Langquan Shui[a], *Yilun Liu*[a, b*], *Xi Chen*[c,d*]

[a] International Center for Applied Mechanics, State Key Laboratory for Strength and Vibration of Mechanical Structure, School of Aerospace, Xi'an Jiaotong University, Xi'an 710049, PR China

[b] Shaanxi Engineering Research Center of Nondestructive Testing and Structural Integrity Evaluation, Xi'an Jiaotong University, Xi'an 710049, PR China

[c] Columbia Nanomechanics Research Center, Department of Earth and Environmental Engineering, Columbia University, New York, NY 10027, USA

[d] School of Chemical Engineering, Northwest University, Xi'an 710069, PR China

Abstract: In this work, Snell's law of elastic waves on the moving property interface (MPI) of time-varying materials has been studied. First, additional constraints of the elastic wave propagation on MPI are proposed to ensure self-consistence of Snell's law. Second, based on Huygens principle, a geometric approach is developed which can be used to geometrically reveal the wave propagation directions on MPI with clear geometric meanings for the additional constraints. Two criteria are proposed to determine the existence of reflected or transmitted wave on MPI. Finally, based on the two criteria, the conditions for the existence of reflected or transmitted waves are expressed by moving velocity of MPI and wave propagation velocities on both sides of MPI. Then, according to the number of reflected and transmitted waves as well as their polarization types, the propagation of elastic wave on MPI can be classified into 6 cases for SH wave incidence, 12 cases for SV wave incidence, and 15 cases for P wave incidence determined by moving velocity of MPI and wave propagation velocities on both sides of MPI. While, the traditional case of elastic wave propagation on a static material interface, i.e. 2 emitted waves for SH wave and 4 emitted waves for SV or P waves are special cases of elastic wave propagation on MPI. It is noted that for most propagation cases presented in this work, the propagation coefficients are unable to be solved with only the continuous conditions on MPI, i.e. the continuity of displacement, stress and momentum on MPI. This work indicates the elastic wave propagation on MPI can have multiple cases of emitted wave which may provide useful insights for further studying elastodynamics of time-varying materials.

Key words: reflection; refraction; snell's law; time-varying materials; elastic waves

* Corresponding author, yilunliu@mail.xjtu.edu.cn (Y.L.); xichen@columbia.edu (X.C.)

1 Introduction

As the rapid growing demand of intelligent materials and structures (for instance, active materials and structures in soft robotics (Hines et al., 2017; Rus and Tolley, 2015)), different types of intelligent materials have been proposed, which can simulate the sensitive and active behaviors of living creatures. In general, these kinds of materials have properties that can be controlled by external applied field, such as temperature, electric field, magnetic field, and laser. For example, the shear resistance of electrorheological (ER) fluid can be controlled by external electrical field. Here, the time-varying materials mentioned in this work are specifically referred to the materials exhibiting rapid time-varying properties to the external fields.

It is of the primary importance to explore the wave propagation behaviors in time-varying materials to promote their applications in intelligent materials and structures (Bergamini et al., 2014; Bogue, 2014; Jakubiak et al., 2003; Jolly et al., 1999; Wang et al., 2016; Wu et al., 2009; Yang and Chen, 2008; Zabow et al., 2015). Reflection and refraction of elastic waves are two common phenomena for elastic wave propagation on material interface with different properties and it seems these phenomena have been well studied for a long-time of research. However, elastic wave propagation in time-varying materials exhibits many new phenomena as indicated by previous literatures of Lurie et al.(Lurie, 2007; Lurie et al., 2009; Lurie and Weekes, 2006), Weekes (2001, 2002, 2003a, b) and Shui et al.(Shui et al., 2017; Shui et al., 2014; Shui et al., 2015). For instance, a SH incident wave propagating on a static material interface has one reflected wave and one transmitted wave, and the propagation directions of the emitted waves are determined by incident angle and wave propagation velocities on both sides of the interface. While, in the time-varying materials, the material interface may move (Shui et al., 2017), which may cause two transmitted waves or no transmitted wave (the evanescent wave is also considered as an emitted wave). Moreover, the propagation directions of the emitted SH waves are not only determined by the incident angle and wave propagation velocities on both sides of the material interface.

Lurie (2007) studied a special case of wave propagation in one dimensional (1-D) case of time-varying materials and found five cases of wave propagation on 1-D MPI (normal incidence), i.e. (a) only one reflected wave, (b) only one transmitted wave, (c) no reflected wave and two transmitted waves, (d) one reflected and one transmitted waves, and (e) one reflected and two transmitted waves. The criteria for the five cases were given. Such results change the insight of elastic wave reflection and refraction on material interface. Shui et al. (2017) further extended the 1-D wave propagation to a general 3-D situation, and also found five cases for SH

wave incidence on MPI. Besides, a classification for the five propagation cases was given in their work, based on which the propagation coefficients of SH wave incidence on MPI is derived. In principle, the classification of propagation cases is the basis for further studying of elastic wave propagation in time-varying materials. However, as the derivation of the velocity criteria of MPI for 3-D wave propagation cases is much more complicated than that of 1-D cases (Shui et al., 2017), especially if SV and P waves are considered, up to now there still lacks the classification of 3-D elastic wave propagation on MPI. Indeed, a smart method should be proposed to consider the potential emitted waves up to seven. Therefore, in this work, we aim to study the Snell's law of 3-D elastic waves on MPI to give the criteria of different propagation cases.

The content of this work is organized as follow. In Section 2, some general descriptions of the Snell's law are presented. In order to ensure self-consistence of the Snell's law, some additional constraints are given. Then, based on Huygens principle, a geometric approach is developed in Section 3, which can significantly simplify the theoretical analysis of wave propagation directions on MPI. Two criteria are given to determine the existence of the reflected or transmitted wave on MPI. Detailed classification of propagation cases for SH waves, SV waves and P waves are given. Finally, conclusions are made in Section 4.

2 General description

In general, the incidence of an elastic wave on static interface formed by two homogenous materials generates constant number of emitted waves. For instance, there must be one reflected wave and one transmitted wave for SH wave incidence, or there must be two reflected waves and two transmitted waves for SV wave incidence. However the number of emitted waves for elastic wave propagation on MPI is varied depending on the moving velocity of MPI and wave velocities on both sides of MPI as shown in previous literatures (Lurie, 2007; Shui et al., 2017; Shui et al., 2014). The moving velocity of MPI has significant influence to the number of emitted waves. If the number of reflected and transmitted waves are unknown, many further discussions (e.g. the propagation coefficients) are impossible. Hence, a clear classification of wave propagation cases on MPI should be given. Since the reflected and transmitted directions are ruled by the Snell's law, the following work is also carried out based on the Snell's law.

For symmetry, the incident and emitted waves propagate in the incident plane. In the incident plane, Shui et al. (2017) have derived the expression of the Snell's law of elastic waves on MPI for isotropic linear elastic media as the following forms:

$$\frac{c_s' - V\cos\alpha^{(T)}}{\sin\alpha^{(T)}} = \frac{c_s - V\cos\alpha^{(R)}}{\sin\alpha^{(R)}} = \frac{c_s - V\cos\alpha^{(I)}}{\sin\alpha^{(I)}} \tag{1a}$$

for SH wave incidence,

$$\frac{c_s' - V\cos\alpha^{(T)}}{\sin\alpha^{(T)}} = \frac{c_s - V\cos\alpha^{(R)}}{\sin\alpha^{(R)}} = \frac{c_l' - V\cos\beta^{(T)}}{\sin\beta^{(T)}} = \frac{c_l - V\cos\beta^{(R)}}{\sin\beta^{(R)}} = \frac{c_s - V\cos\alpha^{(I)}}{\sin\alpha^{(I)}}; \tag{1b}$$

for SV wave incidence and

$$\frac{c_s' - V\cos\alpha^{(T)}}{\sin\alpha^{(T)}} = \frac{c_s - V\cos\alpha^{(R)}}{\sin\alpha^{(R)}} = \frac{c_l' - V\cos\beta^{(T)}}{\sin\beta^{(T)}} = \frac{c_l - V\cos\beta^{(R)}}{\sin\beta^{(R)}} = \frac{c_l - V\cos\beta^{(I)}}{\sin\beta^{(I)}}; \tag{1c}$$

for P wave incidence, where $V \in \mathbf{R}$ is the interface moving velocity induced by material properties changes (Shui et al., 2017). c is the wave propagation velocity (the subscripts "l" and "s" are used to distinguish the wave velocities of the shear and longitudinal waves, respectively (note that $c_l > c_s$). The superscript " ′ " represents the transmitted wave, and the incident and reflected waves are without such mark). The propagation angle α (or β) is defined as the angle between the propagation direction and positive x direction of shear (or longitudinal) waves. The superscripts "(I)", "(R)", and "(T)" are used to distinguish the incident, reflected and transmitted waves, respectively. $\alpha^{(I)}, \beta^{(I)} \in [0, \pi/2]$ for symmetry. Note that the incident and transmission angles are defined as the same as the traditional ones, but the reflection angle defined here is the supplementary angle of the traditional one for convenience of following analysis. By letting $V = 0$, Eq. (1) deduces to the traditional Snell's law. An example of the symbols is illustrated in Fig. 1 by considering SH wave incidence.

Indeed, every solution in Eq. (1) has its reciprocal solution, i.e. $\alpha^{(R)}$ and $\bar{\alpha}^{(R)}$, $\alpha^{(T)}$ and $\bar{\alpha}^{(T)}$, $\beta^{(R)}$ and $\bar{\beta}^{(R)}$, and $\beta^{(T)}$ and $\bar{\beta}^{(T)}$ (if one solution is real, the reciprocal solution is also real; if one solution is complex, the reciprocal solution is its conjugation). Each pair of solution should satisfy (Shui et al., 2017)

$$\left|\mathrm{Re}\left(\alpha^{(R)} - \bar{\alpha}^{(R)}\right)\right|, \left|\mathrm{Re}\left(\alpha^{(T)} - \bar{\alpha}^{(T)}\right)\right|, \left|\mathrm{Re}\left(\beta^{(R)} - \bar{\beta}^{(R)}\right)\right|, \left|\mathrm{Re}\left(\beta^{(T)} - \bar{\beta}^{(T)}\right)\right| \le \pi,$$

and

$$\mathrm{Re}\left(\alpha^{(R)}\right), \mathrm{Re}\left(\bar{\alpha}^{(R)}\right), \mathrm{Re}\left(\alpha^{(T)}\right), \mathrm{Re}\left(\bar{\alpha}^{(T)}\right), \mathrm{Re}\left(\beta^{(R)}\right), \mathrm{Re}\left(\bar{\beta}^{(R)}\right), \mathrm{Re}\left(\beta^{(T)}\right), \mathrm{Re}\left(\bar{\beta}^{(T)}\right) \in \left(-\frac{\pi}{2}, \frac{3}{2}\pi\right).$$

The reciprocal solutions correspond to two conjugate waves with the same velocity and polarization. As the two conjugate waves satisfy the same criteria, the reciprocal solution is omitted for simplification of the expressions. The solution $\alpha^{(R)} = \alpha^{(I)}$ or $\beta^{(R)} = \beta^{(I)}$ corresponds to the incident wave, the solutions $\alpha^{(R)} \neq \alpha^{(I)}$ and $\beta^{(R)} \neq \beta^{(I)}$ correspond to the reflected waves, and the solutions $\alpha^{(T)}$ and $\beta^{(T)}$ correspond to the transmitted waves.

Eq. (1) can be derived from Huygens principle. In Huygens principle, the backward propagations are always ignored. However, as referring to the previous literature (Shui et al., 2017), the backward propagation may exist in time-varying materials, while the forward propagation may disappear. Eq. (1) has several solutions (i.e. 4 solutions for SH waves, or 8 solutions for P or SV waves), and each solution corresponds to one potential propagation direction. Here, it is hard to directly judge the self-consistence of the potential propagation directions due to the different wave phenomena in time-varying materials from that of static materials. Thus, additional constraints are added to Eq. (1) to ensure the self-consistence of Snell's law.

To ensure the incidence of elastic wave to MPI, an incident wave in the downstream of MPI should satisfy

$$c_s \cos\alpha^{(I)}, c_l \cos\beta^{(I)} < V, \tag{2}$$

which means that MPI can catch up the incident wave, and an incident wave in the upstream of MPI should satisfy

$$c_s \cos\alpha^{(I)}, c_l \cos\beta^{(I)} > V, \tag{3}$$

which means that the incident wave can catch up MPI.

For the emitted waves, the travelling wave is considered first. Similarly, to ensure the elastic wave emitting from MPI, an emitted wave in the downstream of MPI should satisfy

$$c_s \cos\alpha^{(R)}, c_s' \cos\alpha^{(T)}, c_l \cos\beta^{(R)}, c_l' \cos\beta^{(T)} \geq V \geq 0 \tag{4a}$$

or

$$c_s \cos\alpha^{(R)}, c_s' \cos\alpha^{(T)}, c_l \cos\beta^{(R)}, c_l' \cos\beta^{(T)} \leq V \leq 0, \tag{4b}$$

which means that MPI cannot catch up the emitted wave; and an emitted wave in the upstream of MPI should satisfy

$$c_s \cos\alpha^{(R)}, c_s' \cos\alpha^{(T)}, c_l \cos\beta^{(R)}, c_l' \cos\beta^{(T)} \leq V \geq 0 \tag{5a}$$

or

$$c_s \cos\alpha^{(R)}, c_s' \cos\alpha^{(T)}, c_l \cos\beta^{(R)}, c_l' \cos\beta^{(T)} \geq V \leq 0, \tag{5b}$$

which means that the emitted wave cannot catch up MPI.

Indeed, the situation of evanescent waves is simpler than that travelling waves. Shui et al. (2017) pointed out that the evanescent wave propagates following with MPI. Thus the relation between the propagation angle and MPI moving velocity V should satisfy one equation, not like the inequalities of Eqs. (4) and (5) for the travelling emitted waves. Based on the attenuation characteristic of the evanescent wave, i.e. the amplitude of the evanescent wave should degenerate zero away from MPI, the reasonable solution for the evanescent wave can be

determined. As a result, if the propagation angle is not real, there must is one and only one determined evanescent wave. Thus, the self-consistence is naturally satisfied. In other words, for evanescent wave, we do not need constraint equations like Eqs. (4) and (5). As can be seen, different constraint conditions are used for travelling and evanescent waves, which is not convenient. Thus, we need constraint equations that can determine reasonable steepest descent direction of the evanescent wave and are compatible with Eqs. (4) and (5) simultaneously. Based on these analyses, the constraint equations are written as

$$\langle c_s \cos\alpha^{(R)}\rangle, \langle c_s' \cos\alpha^{(T)}\rangle, \langle c_l \cos\beta^{(R)}\rangle, \langle c_l' \cos\beta^{(T)}\rangle \geq V \geq 0, \tag{6a}$$

or

$$\langle c_s \cos\alpha^{(R)}\rangle, \langle c_s' \cos\alpha^{(T)}\rangle, \langle c_l \cos\beta^{(R)}\rangle, \langle c_l' \cos\beta^{(T)}\rangle \leq V \leq 0, \tag{6b}$$

when an emitted wave is in the downstream of MPI; and

$$\langle c_s \cos\alpha^{(R)}\rangle, \langle c_s' \cos\alpha^{(T)}\rangle, \langle c_l \cos\beta^{(R)}\rangle, \langle c_l' \cos\beta^{(T)}\rangle \leq V \geq 0, \tag{7a}$$

or

$$\langle c_s \cos\alpha^{(R)}\rangle, \langle c_s' \cos\alpha^{(T)}\rangle, \langle c_l \cos\beta^{(R)}\rangle, \langle c_l' \cos\beta^{(T)}\rangle \geq V \leq 0, \tag{7b}$$

when an emitted wave is in the upstream of MPI. The operator $\langle\cdot\rangle = \mathrm{Re}(\cdot) + \mathrm{Im}(\cdot)$. Eqs. (4) and (5) can be deduced from Eqs. (6) and (7). In deriving Eqs. (6) and (7), two direction vectors, $\left(\mathrm{Re}\left(\cos\alpha^{(T)}\right), \mathrm{Re}\left(\sin\alpha^{(T)}\right)\right)$ and $\left(\mathrm{Im}\left(\cos\alpha^{(T)}\right), \mathrm{Im}\left(\sin\alpha^{(T)}\right)\right)$ are used. Direction of the first vector is the propagation direction of the traveling wave component of the evanescent wave, and direction of the second vector is the steepest descent direction of the evanescent wave. To get better understanding of Eqs. (6) and (7), one can refer to Section 3.1, where the example in Fig. 2(f) demonstrates that the x-component of the vectors $\overrightarrow{OT^{(T)}}$ and $\overrightarrow{O\bar{T}^{(T)}}$ are just $\langle c_s' \cos\alpha^{(T)}\rangle$ and $\langle c_s' \cos\bar{\alpha}^{(T)}\rangle$, one is not less than V, and the other one is not greater than V. Eqs. (2) to (7) can be combined and simplified as

$$\left(c_s \cos\alpha^{(I)} - V\right)\left(\langle c_s \cos\alpha^{(R)}\rangle - V\right) \leq 0, \left(V \neq c_s \cos\alpha^{(I)}\right), \tag{8a}$$

$$\left(c_s \cos\alpha^{(I)} - V\right)\left(\langle c_l \cos\beta^{(R)}\rangle - V\right) \leq 0, \left(V \neq c_s \cos\alpha^{(I)}\right), \tag{8b}$$

$$\left(c_l \cos\beta^{(I)} - V\right)\left(\langle c_s \cos\alpha^{(R)}\rangle - V\right) \leq 0, \left(V \neq c_l \cos\beta^{(I)}\right), \tag{8c}$$

$$\left(c_l \cos\beta^{(I)} - V\right)\left(\langle c_l \cos\beta^{(R)}\rangle - V\right) \leq 0, \left(V \neq c_l \cos\beta^{(I)}\right); \tag{8d}$$

and

$$\left(c_s \cos\alpha^{(I)} - V\right)\left(\langle c_s' \cos\alpha^{(T)}\rangle - V\right) \geq 0, \left(V \neq c_s \cos\alpha^{(I)}\right), \tag{9a}$$

$$\left(c_s \cos\alpha^{(I)} - V\right)\left(\langle c_l' \cos\beta^{(T)}\rangle - V\right) \geq 0, \left(V \neq c_s \cos\alpha^{(I)}\right), \tag{9b}$$

$$\left(c_l \cos\beta^{(I)} - V\right)\left(\langle c_s' \cos\alpha^{(T)}\rangle - V\right) \geq 0, \left(V \neq c_l \cos\beta^{(I)}\right), \tag{9c}$$

$$\left(c_l \cos\beta^{(I)} - V\right)\left(\langle c_l' \cos\beta^{(T)}\rangle - V\right) \geq 0, \left(V \neq c_l \cos\beta^{(I)}\right). \tag{9d}$$

Eqs. (8) and (9) give the additional constraint equations that the reflected and transmitted waves should satisfy.

Combining Eqs. (1), (8) and (9), the complete Snell's law of elastic wave propagation on MPI is given. It can be seen that such form of Snell's law is still implicit and not convenient to distinguish the propagation cases on MPI. To directly obtain the wave propagation directions that satisfy the self-consistence, a geometric approach is developed in Section 3.

3 Classification of wave propagation cases

3.1 Method

In principle, the self-consistent wave propagation directions can be obtained by directly solving Eqs. (1) to (3), (8) and (9), i.e. the complete Snell's law of elastic wave propagation on MPI. However, only for the reflected wave with the same polarization to that of the incident wave, its solution can be explicitly given as

$$\alpha^{(R)} = 2\arctan\left(\frac{c_s - V}{c_s + V}\cot\frac{\alpha^{(I)}}{2}\right)\left(|V| < c_s \text{ and } V \neq c_s\cos\alpha^{(I)}\right), \tag{10a}$$

$$\beta^{(R)} = 2\arctan\left(\frac{c_l - V}{c_l + V}\cot\frac{\beta^{(I)}}{2}\right)\left(|V| < c_l \text{ and } V \neq c_l\cos\beta^{(I)}\right). \tag{10b}$$

For other propagation cases, the equations need to be numerically solved. In this work, we developed a geometric approach to represent the complete Snell's law and deduce the classification of wave propagation cases in a more convenient and intuitional way.

Solutions of Eq. (1) can be expressed geometrically based on Huygens principle. The equality of the first and last item in Eq. (1c), which describes P wave incidence and SV wave transmission, is demonstrated as an example ($\left(c_s' - V\cos\alpha^{(T)}\right)/\sin\alpha^{(T)} = \left(c_l - V\cos\beta^{(I)}\right)/\sin\beta^{(I)}$). The procedures of the geometric approach and its meanings (the geometric approach can be strictly proved to equivalence with those of Eqs. (1), (8) and (9)) are presented as following:

Step 1: draw two circles with center positions at Origin point O and radiuses of c_l and c_s', denoted as $\odot O_l$ and $\odot O_s'$, respectively. $\odot O_l$ and $\odot O_s'$ represent the two wave fronts with wave velocities c_l and c_s' emitted from Origin point O after a unit time, respectively. $\odot O_l$ is the black circle corresponding to the incident wave; $\odot O_s'$ is the blue circle corresponding to emitted wave, as shown in Fig. 2(a).

Step 2: draw a line A_0A (the red line in Fig. 2(b)) through $A_0(V, 0)$ and parallel to y-axis. A_0A

represents the location of MPI from the Origin point O after a unit time.

Step 3: draw a line segment $OT^{(I)}$ intersecting with $\odot O_l$ at $T^{(I)}$, let the angle between $\overrightarrow{OT^{(I)}}$ and positive x direction be the incident angle $\beta^{(I)}$. The direction of $\overrightarrow{OT^{(I)}}$ represents the propagation direction of the incident wave, see Fig. 2(c).

Step 4: draw a tangent line of $\odot O_l$ at $T^{(I)}$ and intersecting with line A_0A at A, see Fig. 2(d).

Step 5 (case 1): point A is on the outer side of $\odot O_s'$. The emitted wave is travelling wave. Draw a tangent line of $\odot O_s'$ through A and $T^{(T)}$ ($\bar{T}^{(T)}$) on $\odot O_s'$. The direction of $\overrightarrow{OT^{(T)}}$ ($\overrightarrow{O\bar{T}^{(T)}}$) represents the propagation direction of transmitted wave, and the angle between $\overrightarrow{OT^{(T)}}$ ($\overrightarrow{O\bar{T}^{(T)}}$) and positive x direction is $\alpha^{(T)}$ ($\bar{\alpha}^{(T)}$), see Fig. 2(e).

Step 5 (case 2): point A is on the inner side of $\odot O_s'$. The emitted wave is evanescent wave. Draw a isometric hyperbola and let its vertexes locate at the intersections between line OA and $\odot O_s'$; draw a tangent line of the hyperbola passing through A and $T^{(T)}$ ($\bar{T}^{(T)}$) on the hyperbola. Connect points $T^{(T)}$ and $\bar{T}^{(T)}$; line segment $T^{(T)}\bar{T}^{(T)}$ intersects with line OA at B. $\overrightarrow{OA} = (V, c_{0i}\csc\alpha_{0i} - V\cot\alpha_{0i})$, and the direction and length of $\overrightarrow{OA}$ represent the propagation direction and speed of the traveling wave component of the evanescent wave, respectively; the angle between $\overrightarrow{OA}$ and positive x direction is $\mathrm{Re}(\alpha^{(T)})$; the area of the orange region $T^{(T)}O\bar{T}^{(T)}$ (scaled hyperbolic angle) is $c_s'^2\left|\mathrm{Im}(\alpha^{(T)})\right|$, which determines the exponential decay rate of the evanescent wave; $\overrightarrow{OB} = c_s'\left(\mathrm{Re}(\cos\alpha^{(T)}), \mathrm{Re}(\sin\alpha^{(T)})\right)$, $\overrightarrow{BT^{(T)}} = c_s'\left(\mathrm{Im}(\cos\alpha^{(T)}), \mathrm{Im}(\sin\alpha^{(T)})\right)$, and the direction of $\overrightarrow{BT^{(T)}}$ or $\overrightarrow{B\bar{T}^{(T)}}$ is the steepest descent direction of the corresponding evanescent wave, see Fig. 2(f).

Based on the geometrical approach mentioned above (Fig. 2), Eq. (1) can be geometrically solved. The additional constraint equations of Eqs. (8) and (9) can be described by x-coordinate of $\overrightarrow{OT^{(R)}}$, $\overrightarrow{OT^{(T)}}$ and V. First, it should be noted that if $T^{(I)}$ is at line AA_0, there are not emitted waves as the incident wave cannot meet MPI. Eq. (8) means that points $T^{(I)}$ and $T^{(R)}$ should be at different sides of line AA_0, or point $T^{(R)}$ is at line AA_0. On the other hand, Eq. (9) means that both points $T^{(I)}$ and $T^{(T)}$ should be at the same side of AA_0, or point $T^{(T)}$ is at line AA_0. In addition, as indicated by Fig. 2, the basic geometric relationships of the related points and lines are still valid if the solution of Eq. (1) is complex. Thus, it is not necessary to treat the propagation cases of evanescent waves individually. Two criteria are summarized as follow:

Criterion I: ***Criterion for reflected waves****: points* $T^{(I)}$ *and* $T^{(R)}$ *are at different sides of line* AA_0*, or point* $T^{(R)}$ *is at line* AA_0 *(*$T^{(I)}$ *cannot be at line* AA_0*).*

Criterion II: ***Criterion for transmitted waves****: both points* $T^{(I)}$ *and* $T^{(T)}$ *are at the same side of* AA_0*, or point* $T^{(T)}$ *is at line* AA_0 *(*$T^{(I)}$ *cannot be at line* AA_0*).*

To illustrate applicability of the two criteria, the 1-D situation (Lurie, 2007; Shui et al., 2014) is analyzed as an example (considering normal incidence of SH wave). As introduced in Section 1, Lurie (2007) found five cases of wave propagation on 1-D MPI, e.g. there will be one reflected and two transmitted waves for $-c_s \le V \le -c_s'$. Specifically, for the 1-D situation ($\alpha^{(I)} \to 0$), the solutions of Eq. (1a) should degenerate to 0 and π. The geometric demonstration is given in Fig. 3. When $\alpha^{(I)} \to 0$, the location of point A is at the positive infinite. Thus, the four tangent points ($T^{(I)}$, $T^{(R)}$, $T^{(T)}$, $\bar{T}^{(T)}$) should be intersections of the circles and x-axis, and the evanescent wave cannot exist. Fig. 3(a) demonstrates the traditional situation of static material interface ($V = 0$). The MPI AA_0 is through the Origin. By **Criterion I**, the reflected wave with $T^{(R)}$ is self-consistent. By **Criterion II**, the transmitted wave with $\bar{T}^{(T)}$ is self-consistent. However, the transmitted wave with $T^{(T)}$ is not self-consistent. Thus, there is one reflected wave and one transmitted wave, which is in consistent with the well-known phenomenon of static material interface. Fig. 3(b) demonstrates the case $-c_s \le V \le -c_s'$. By **Criterion I**, the reflected wave with $T^{(R)}$ is self-consistent. By **Criterion II**, the transmitted waves with $\bar{T}^{(T)}$ and $T^{(T)}$ are self-consistent. Thus, there should be one reflected and two transmitted waves, which is in consistent with previous results of MPI (Lurie, 2007; Shui et al., 2014).

Based on above method, the complete Snell's law of elastic wave propagation on MPI can be illustrated geometrically, and the propagation cases can be easily distinguished based on the moving velocity of MPI and incident angle. The detailed self-consistent propagation cases for SH, P and SV waves are given in following sections. Before further discussion, we introduce a series of symbols, $\mathbf{D}_{s\to l}^{(R\times i)}$, $\mathbf{D}_{s\to s}^{(R\times i)}$, $\mathbf{D}_{l\to l}^{(R\times i)}$, $\mathbf{D}_{l\to s}^{(R\times i)}$, $\mathbf{D}_{s\to l}^{(T\times i)}$, $\mathbf{D}_{s\to s}^{(T\times i)}$, $\mathbf{D}_{l\to l}^{(T\times i)}$, $\mathbf{D}_{l\to s}^{(T\times i)}$. Illustrating by an example, the first one, $\mathbf{D}_{s\to l}^{(R\times i)}$, represents a set of V for the existence of i reflected longitudinal waves induced by shear wave incidence. "i" is the number of existed waves which can be 0, 1, and 2. For the evanescent waves, "i" should be "1", it is specially replaced by "e" for convenience.

3.2 Classification of the propagation cases of SH waves

For SH incident wave, Eq. (1) has two pairs of solutions, and there are maximum one reflected wave and two transmitted waves. It can be verified that the set of V for one reflected wave should be (Fig. 4(a))

$$\mathbf{D}_{S\to S}^{(R\times 1)} = \{V||V| \le c_s, V \ne c_s \cos\alpha^{(I)}\}, \tag{11}$$

and the reflected wave cannot be an evanescent wave because point A must be at the outer side of $\odot O_s$. Obviously, the set for no transmitted wave should be (Fig. 4(b))

$$\mathbf{D}_{S\to S}^{(R\times 0)} = \mathbf{R}\backslash\mathbf{D}_{S\to S}^{(R\times 1)}, \tag{12}$$

where $\mathbf{R}$ is the real domain.

According to the criterion of transmitted waves (**Criterion II**), if there are no or two transmitted waves, points $T^{(T)}$ and $\bar{T}^{(T)}$ should be at the same side of line AA_0 or point $T^{(T)}$ or $\bar{T}^{(T)}$ is at line AA_0. Thus, AA_0 is separated by $\odot O_s'$ or tangent to $\odot O_s'$ (Fig. 5), which gives that

$$|V| \ge c_s'. \tag{13}$$

Because $OT^{(I)} \perp AT^{(I)}$, $T^{(I)}$ should be at a circle with diameter AO (the red dash-dotted lines). Considering that $\alpha^{(I)} \in [0, \pi/2]$, part of the circle is deleted, and the red arcs is left in Fig. 5.

According to **Criterion II**, if there are two transmitted waves, points $T^{(T)}$, $\bar{T}^{(T)}$ and $T^{(I)}$ should at the same side of line AA_0. Therefore, $T^{(I)}$ should be at arc $\widehat{\mathrm{AP}}$) in Fig. 5(a) or arc $\widehat{\mathrm{OP}}$) in Fig. 5(b). In Fig. 5(a), $V \ge c_s'$, the condition $0 \le c_s \cos\alpha^{(I)} \le V$ should be satisfied to let $\alpha^{(I)}$ be at arc $\widehat{\mathrm{AP}}$). In Fig. 5(b), $V \le -c_s'$, $\forall\alpha^{(I)} \in [0, \pi/2]$, there are two transmitted waves. Thus the set for two transmitted wave should be

$$\mathbf{D}_{S\to S}^{(T\times 2)} = \{V|V \le -c_s'\} \cup \{V|V \ge \max\{c_s \cos\alpha^{(I)}, c_s'\}, V \ne c_s \cos\alpha^{(I)}\}. \tag{14}$$

These two transmitted waves cannot be evanescent waves because point A must be at the outer side of $\odot O_s'$.

For the propagation cases without transmitted wave, points $T^{(T)}$ and $\bar{T}^{(T)}$, and $T^{(I)}$ should be at different sides of line AA_0. Consequently, only if $V \ge c_s'$, and $T^{(I)}$ is at arc $\mathrm{AA}\overset{\frown}{}_0$?)) (Fig. 5(a)), there is not transmitted wave, so the condition $c_s \cos\alpha^{(I)} \ge V$ should be satisfied. Hence, the set for no transmitted wave should be

$$\mathbf{D}_{S\to S}^{(T\times 0)} = \{V|c_s' < V \le c_s \cos\alpha^{(I)}\}; \tag{15}$$

For the propagation case with one transmitted wave, points $T^{(T)}$ and $\bar{T}^{(T)}$ should at different sides of line AA_0, and $T^{(T)}$ and $\bar{T}^{(T)}$ cannot be at line AA_0. As a result, the set for

one transmitted wave should be (Fig. 6)

$$\mathbf{D}_{s\to s}^{(T\times 1)} = \left\{V \middle| |V| < c_s', V \neq c_s \cos\alpha^{(I)}\right\}. \tag{16}$$

The transmitted wave in this case can be an evanescent wave if points A is at chord BC except $T^{(I)}$ (Fig. 6). It can be derived that the set for the existence of evanescent wave is

$$\mathbf{D}_{s\to s}^{(T\times e)} = \left\{V \middle| c_s \cos\alpha^{(I)} - \sqrt{c_s'^2 - c_s^2}\sin\alpha^{(I)} \le V \le c_s \cos\alpha^{(I)} + \sqrt{c_s'^2 - c_s^2}\sin\alpha^{(I)} \sin\alpha_{01}, V \neq c_s \cos\alpha^{(I)}\right\} \subset \mathbf{D}_{s\to s}^{(T\times 1)}, (c_s < c_s'). \tag{17}$$

By intersection operation of the sets for the existence of the reflected or transmitted waves (column 4 in Table 1), the classification of the propagation cases of SH waves on MPI are listed in Table 1 in consistent with previous work (Shui et al., 2017) and schematically demonstrated in Fig. 7. It can be verified that the ranges of V listed in Table 1 completely cover the real domain without overlapping. The propagation scenarios shown in Fig. 7 agree with the previous simulation results (Shui et al., 2017). It can be seen from Fig. 7(e) that case SH-v is similar to the classic wave propagation on static material interface. For the propagation coefficients, except cases of SH-iii and SH-v which have only two emitted waves, the propagation coefficients cannot solved by the two continuous conditions, i.e. the displacement, stress and momentum continuity on MPI due to the inequality of unknown variables and equations. To obtain the propagation coefficients for all propagation cases, a method based on weak solutions of the continuity should be developed (Shui et al., 2017).

3.3 Classification of the propagation cases of SV and P waves

When the incident wave is SV or P waves, the emitted waves are always both SV and P waves. For the emitted waves with the same polarization to the incident wave, the propagation cases are similar to that of SH waves as discussed in Section 3.2. It is noted that P waves always propagate faster than SV waves. Actually, the ratio of P wave velocity to SV wave velocity is

$$\frac{c_l}{c_s} = \sqrt{\frac{2-2\nu}{1-2\nu}} > \sqrt{\frac{4}{3}} > 1 \tag{18}$$

as Poisson ratio $\nu \in (-1, 0.5)$. Such relation should be considered in the analysis. Thus, the propagation cases for emitted waves with different polarizations from that of the incident wave are different. The general analysis in this section is similar to that in Section 3.2, but the classification for P or SV waves incidence are much more complicated.

3.3.1 Reflected waves

Firstly, for the reflected wave with the same polarization to the incident wave, the

propagation cases are similar to that of SH waves, and the set of the reflected wave should be

$$\mathbf{D}_{s\to s}^{(R\times 1)} = \{V||V| \le c_s, V \ne c_s \cos\alpha^{(I)}\}, \tag{19a}$$

$$\mathbf{D}_{l\to l}^{(R\times 1)} = \{V||V| \le c_l, V \ne c_l \cos\beta^{(I)}\}. \tag{19b}$$

The reflected wave cannot be an evanescent wave because point A must be at the outer side of $\odot O_s$ or $\odot O_l$. Similarly, the set of zero reflected wave is

$$\mathbf{D}_{s\to s}^{(R\times 0)} = \mathbf{R}\backslash\mathbf{D}_{s\to s}^{(R\times 1)}, \tag{20a}$$

$$\mathbf{D}_{l\to l}^{(R\times 0)} = \mathbf{R}\backslash\mathbf{D}_{l\to l}^{(R\times 1)}. \tag{20b}$$

Therefore, we focused on the reflected waves with different polarizations from the incident wave. According to the criterion for reflected waves (**Criterion I**), if there are zero or two reflected waves, points $T^{(R)}$ and $\overline{T}^{(R)}$ should at the same side of line AA_0. Such cases are similar to the transmitted waves analyzed in Section 3.2. The difference is that the criteria are opposite. Therefore, it can be derived that the sets of MPI moving velocity V for the reflected waves with different polarizations from the incident wave should be

$$\mathbf{D}_{s\to l}^{(R\times 0)} = \{V|V < -c_l\} \cup \{V|V > \max\{c_s \cos\alpha^{(I)}, c_l\}\} \cup \{V|V = c_s \cos\alpha^{(I)}\}, \tag{21a}$$

$$\mathbf{D}_{l\to s}^{(R\times 0)} = \{V|V < -c_s\} \cup \{V|V > \max\{c_l \cos\beta^{(I)}, c_s\}\} \cup \{V|V = c_l \cos\beta^{(I)}\}; \tag{21b}$$

$$\mathbf{D}_{s\to l}^{(R\times 1)} = \{V||V| \le c_l, V \ne c_s \cos\alpha^{(I)}\}, \tag{22a}$$

$$\mathbf{D}_{l\to s}^{(R\times 1)} = \{V||V| \le c_s, V \ne c_l \cos\beta^{(I)}\}; \tag{22b}$$

$$\mathbf{D}_{s\to l}^{(R\times 2)} = \{V|c_l < V < c_s \cos\alpha^{(I)}\}, \tag{23a}$$

$$\mathbf{D}_{l\to s}^{(R\times 2)} = \{V|c_s < V < c_l \cos\beta^{(I)}\}. \tag{23b}$$

As $c_l > c_s$ (Eq. (18)), the reflected wave cannot be evanescent wave if the incident wave is P wave. If the incident wave is SV wave and $V \in \mathbf{D}_{s\to l}^{(R\times 1)}$, the reflected wave can be an evanescent wave as $c_l > c_s$ (Eq. (18)), and the set for evanescent wave should be

$$\mathbf{D}_{s\to l}^{(R\times e)} = \left\{V|c_s \cos\alpha^{(I)} - \sqrt{c_l^2 - c_s^2}\sin\alpha^{(I)} \le V \le c_s \cos\alpha^{(I)} + \sqrt{c_l^2 - c_s^2}\sin\alpha^{(I)}, V \ne c_s \cos\alpha^{(I)}\right\} \subset \mathbf{D}_{s\to l}^{(R\times 1)}, (c_s < c_l). \tag{24}$$

3.3.2 Transmitted waves

Similar to the results of SH wave incidence, the sets for transmitted waves can be derived as

$$\mathbf{D}_{s\to s}^{(T\times 0)} = \{V|c_s' < V \le c_s \cos\alpha^{(I)}\}, \tag{25a}$$

$$\mathbf{D}_{s\to l}^{(T\times 0)} = \{V|c_l' < V \le c_s \cos\alpha^{(I)}\}, \tag{25b}$$

$$\mathbf{D}_{l\to s}^{(T\times 0)} = \{V | c_s' < V \le c_l \cos\beta^{(I)}\}, \tag{25c}$$

$$\mathbf{D}_{l\to l}^{(T\times 0)} = \{V | c_l' < V \le c_l \cos\beta^{(I)}\}; \tag{25d}$$

$$\mathbf{D}_{s\to s}^{(T\times 1)} = \{V | |V| < c_s', V \ne c_s \cos\alpha^{(I)}\}, \tag{26a}$$

$$\mathbf{D}_{s\to l}^{(T\times 1)} = \{V | |V| < c_l', V \ne c_s \cos\alpha^{(I)}\}, \tag{26b}$$

$$\mathbf{D}_{l\to s}^{(T\times 1)} = \{V | |V| < c_s', V \ne c_l \cos\beta^{(I)}\}, \tag{26c}$$

$$\mathbf{D}_{l\to l}^{(T\times 1)} = \{V | |V| < c_l', V \ne c_l \cos\beta^{(I)}\}; \tag{26d}$$

$$\mathbf{D}_{s\to s}^{(T\times 2)} = \{V | V \le -c_s'\} \cup \left\{V | V \ge \max\left\{c_s \cos\alpha^{(I)}, c_s'\right\}, V \ne c_s \cos\alpha^{(I)}\right\}, \tag{27a}$$

$$\mathbf{D}_{s\to l}^{(T\times 2)} = \{V | V \le -c_l'\} \cup \left\{V | V \ge \max\left\{c_s \cos\alpha^{(I)}, c_l'\right\}, V \ne c_s \cos\alpha^{(I)}\right\}, \tag{27b}$$

$$\mathbf{D}_{l\to s}^{(T\times 2)} = \{V | V \le -c_s'\} \cup \left\{V | V \ge \max\left\{c_l \cos\beta^{(I)}, c_s'\right\}, V \ne c_l \cos\beta^{(I)}\right\}, \tag{27c}$$

$$\mathbf{D}_{l\to l}^{(T\times 2)} = \{V | V \le -c_l'\} \cup \left\{V | V \ge \max\left\{c_l \cos\beta^{(I)}, c_l'\right\}, V \ne c_l \cos\beta^{(I)}\right\}; \tag{27d}$$

$$\mathbf{D}_{s\to s}^{(T\times e)} = \left\{V | c_s \cos\alpha^{(I)} - \sqrt{c_s'^2 - c_s^2}\sin\alpha^{(I)} \le V \le c_s \cos\alpha^{(I)} + \sqrt{c_s'^2 - c_s^2}\sin\alpha^{(I)}, V \ne c_s \cos\alpha^{(I)}\right\} \subset \mathbf{D}_{s\to s}^{(T\times 1)}, (c_s < c_s'), \tag{28a}$$

$$\mathbf{D}_{s\to l}^{(T\times e)} = \left\{V | c_s \cos\alpha^{(I)} - \sqrt{c_l'^2 - c_s^2}\sin\alpha^{(I)} \le V \le c_s \cos\alpha^{(I)} + \sqrt{c_l'^2 - c_s^2}\sin\alpha^{(I)}, V \ne c_s \cos\alpha^{(I)}\right\} \subset \mathbf{D}_{s\to s}^{(T\times 1)}, (c_s < c_l'), \tag{28b}$$

$$\mathbf{D}_{l\to s}^{(T\times e)} = \left\{V | c_l \cos\beta^{(I)} - \sqrt{c_s'^2 - c_l^2}\sin\beta^{(I)} \le V \le c_l \cos\beta^{(I)} + \sqrt{c_s'^2 - c_l^2}\sin\beta^{(I)}, V \ne c_l \cos\beta^{(I)}\right\} \subset \mathbf{D}_{l\to s}^{(T\times 1)}, (c_l < c_s'), \tag{28c}$$

$$\mathbf{D}_{l\to l}^{(T\times e)} = \left\{V | c_l \cos\beta^{(I)} - \sqrt{c_l'^2 - c_l^2}\sin\beta^{(I)} \le V \le c_l \cos\beta^{(I)} + \sqrt{c_l'^2 - c_l^2}\sin\beta^{(I)}, V \ne c_l \cos\beta^{(I)}\right\} \subset \mathbf{D}_{l\to s}^{(T\times 1)}, (c_l < c_l'). \tag{28d}$$

It is noted that if point A is at chord BC of $\odot O_s'$ (Fig. 6), A must be at the inner side of $\odot O_l'$ (Eq. (18)), which means that if the transmitted SV wave is an evanescent wave, the transmitted P wave must also be an evanescent wave.

3.3.3 Classification of the propagation cases

The classification of the propagation cases is actually the set operation of $\mathbf{D}$ under the constraint of Eq. (18). For instance, for the case of SV wave incidence with i reflected SV waves,

j reflected P waves, k transmitted SV waves, and l transmitted P waves, set of the MPI moving V should be $\mathbf{D}_{S\to S}^{(R\times i)} \cap \mathbf{D}_{S\to l}^{(R\times j)} \cap \mathbf{D}_{S\to S}^{(T\times k)} \cap \mathbf{D}_{S\to l}^{(T\times l)} (i = 0,1; j = 0,1,2; k = 0,1,2; l = 0,1,2)$ (similar to column 4 in Table 1). Thus, there are maximum $54 \times 2 = 108$ kinds of propagation cases for SV wave or P wave incidence by considering different numbers of emitted waves and different polarizations. However, the final results are not so complicated because most cases are inexistence as the corresponding sets of the MPI moving V are empty. Indeed, at most 27 kinds of propagation cases are distinguished. The classification of propagation cases of SV and P waves are listed in Table 2 and Table 3, and schematically demonstrated in Fig. 8 and Fig. 9, respectively. The propagation characteristics of cases P-i ~ P-xii are quite similar to that of SV wave incidence for case SV-i ~ SV-xii (referring to Table 2 and Table 3), and the only difference is the absence of evanescent waves, thus the propagation cases P-i ~ P-xii are not demonstrated, i.e. only cases P-xiii ~ P-xv are demonstrated in Fig. 9. It can be verified that the ranges of V listed in Table 2 (or Table 3) completely cover the real domain without overlapping. It can be seen from Fig. 8(j) that case SV-x (or P-x) is similar to the traditional wave propagation on static material interface. For the propagation coefficients, except cases SV-iv, SV-vi, SV-x, P-iv, P-vi, P-x, and P-xv, which have four emitted waves, the propagation coefficients for other propagation cases are not solvable with the four continuous conditions of displacement, stress and momentum on MPI due to the inequality of unknown variables and equations. To obtain the propagation coefficients for all propagation cases, a method based on weak solutions of the continuity on MPI should be considered (Shui et al., 2017).

4 Conclusion

In this work, based on Huygens principle, a geometric approach is proposed to study the Snell's law of elastic wave propagation on MPI. Two criteria are proposed to determine the existence of the reflected and transmitted wave. Based on the criteria, 6 types of SH wave, 12 types of SV, and 15 types of P wave propagation cases are found, and the corresponding sets of MPI moving velocity V are obtained. It is noted that the propagation coefficients for most propagation cases can not directly solved by continuous conditions of displacement, stress and momentum on MPI due to the inequality of unknown variables and equations. The geometric approach presented in this work is a convenient, simple and intuitive method to predict the number and direction of the emitted waves for elastic wave propagation on MPI. The results show complex characteristics of wave propagation on MPI, which may provide useful insights for further studying the elastodynamics of time-varying materials and time-varying structural

composites.

Acknowledgements

Y.L. acknowledges the support from the National Natural Science Foundation of China (No. 11572239). X.C. acknowledges the support from the National Natural Science Foundation of China (Nos. 11372241 and 11572238), ARPA-E (DE-AR0000396) and AFOSR (FA9550-12-1-0159).

Reference

Bergamini, A., Delpero, T., De Simoni, L., Di Lillo, L., Ruzzene, M., Ermanni, P., 2014. Phononic Crystal with Adaptive Connectivity. Adv Mater 26, 1343-1347.

Bogue, R., 2014. Smart materials: a review of capabilities and applications. Assembly Autom 34, 16-22.

Hines, L., Petersen, K., Lum, G.Z., Sitti, M., 2017. Soft Actuators for Small-Scale Robotics. Adv Mater 29, 1603483.

Jakubiak, R., Bunning, T.J., Vaia, R.A., Natarajan, L.V., Tondiglia, V.P., 2003. Electrically switchable, one-dimensional polymeric resonators from holographic photopolymerization: A new approach for active photonic bandgap materials. Adv Mater 15, 241-244.

Jolly, M.R., Bender, J.W., Carlson, J.D., 1999. Properties and applications of commercial magnetorheological fluids. J Intel Mat Syst Str 10, 5-13.

Lurie, K.A., 2007. An Introduction to the Mathematical Theory of Dynamic Materials, Springer, New York, 2007 .

Lurie, K.A., Onofrei, D., Weekes, S.L., 2009. Mathematical analysis of the waves propagation through a rectangular material structure in space-time. J Math Anal Appl 355, 180-194.

Lurie, K.A., Weekes, S.L., 2006. Wave propagation and energy exchange in a spatio-temporal material composite with rectangular microstructure. J Math Anal Appl 314, 286-310.

Rus, D., Tolley, M.T., 2015. Design, fabrication and control of soft robots. Nature 521, 467-475.

Shui, L.Q., Liu, Y.L., Chen, X., 2017. Three dimensional wave propagation in time-varying materials: A mathematical model based on the weak solutions of continuity in the moving property interface. Applied Mathematical Modelling 48, 134-152.

Shui, L.Q., Yue, Z.F., Liu, Y.S., Liu, Q.C., Guo, J.J., 2014. One-dimensional linear elastic waves at

moving property interface. Wave Motion 51, 1179-1192.

Shui, L.Q., Yue, Z.F., Liu, Y.S., Liu, Q.C., Guo, J.J., He, X.D., 2015. Novel composites with asymmetrical elastic wave properties. Compos Sci Technol 113, 19-30.

Wang, Z.W., Zhang, Q., Zhang, K., Hu, G.K., 2016. Tunable Digital Metamaterial for Broadband Vibration Isolation at Low Frequency. Adv Mater 28, 9857-9861.

Weekes, S.L., 2001. Numerical computation of wave propagation in dynamic materials. Appl Numer Math 37, 417-440.

Weekes, S.L., 2002. A stable scheme for the numerical computation of long wave propagation in temporal laminates. J Comput Phys 176, 345-362.

Weekes, S.L., 2003a. Dispersion effects in dynamic laminates. Physica B 338, 64-66.

Weekes, S.L., 2003b. A dispersive effective equation for wave propagation through spatio-temporal laminates. Wave Motion 38, 25-41.

Wu, L.Y., Wu, M.L., Chen, L.W., 2009. The narrow pass band filter of tunable 1D phononic crystals with a dielectric elastomer layer. Smart Mater Struct 18, 015011.

Yang, W.P., Chen, L.W., 2008. The tunable acoustic band gaps of two-dimensional phononic crystals with a dielectric elastomer cylindrical actuator. Smart Mater Struct 17, 015011.

Zabow, G., Dodd, S.J., Koretsky, A.P., 2015. Shape-changing magnetic assemblies as high-sensitivity NMR-readable nanoprobes. Nature 520, 73-77.

Figure Legends

Fig. 1 Symbol illustration of waves in the incident plane: an example considering SH wave incidence. $V \in \boldsymbol{R}$ is the interface moving velocity induced by material properties changes (Shui et al., 2017). The propagation angle α (or β) is defined as the angle between the propagation direction and positive x direction of shear (or longitudinal) waves. The superscripts "(I)", "(R)", and "(T)" are used to distinguish the incident, reflected and transmitted waves, respectively. $\alpha^{(I)}, \beta^{(I)} \in [0, \pi/2]$ for symmetry. Note that the incident and transmission angles are defined as the same as the traditional ones, but the reflection angle defined here is the supplementary angle of the traditional one.

Fig. 2 Illustration of the geometric analysis method of Snell's law on MPI. (a) step 1; (b) step 2; (c) step 3; (d) step 4; (e) step 5 (case 1), demonstration of a travelling wave ($\alpha^{(T)} \in \mathbf{R}$); and (f) step 5 (case 2), demonstration of an evanescent wave ($\alpha^{(T)} \in \mathbf{Z/R}$). The blue elements correspond to the emitted waves, and the black ones correspond to the incident wave. (For interpretation of the references to color in this figure legend, the reader is referred to the web version of this article)

Fig. 3 Examples of the geometric approach: (a) common situation with static material interface (V=0). **Criterion (1)** indicates that the reflected wave with $T^{(R)}$ is self-consistent. **Criterion (2)** indicates that the transmitted wave with $\bar{T}^{(T)}$ is self-consistent, however the transmitted wave with $T^{(T)}$ is not self-consistent. Thus, there is one reflected wave and one transmitted wave, which is in line with the well-known phenomenon; (b) the case with $-c_s \le V \le -c_s'$. **Criterion (1)** and **(2)** indicate that all the reflected wave with $T^{(R)}$, transmitted wave with $\bar{T}^{(T)}$ and $T^{(T)}$ are self-consistent. Thus, there should be one reflected and two transmitted waves, which is in line with previous results (Lurie, 2007; Shui et al., 2014). The solid lines with arrow mean self-consistent reflected waves and the dotted line with arrow means self-inconsistent reflected wave which should not exist during the practical propagation of SH wave on MPI.

Fig. 4 Geometric demonstration of the reflected SH waves: (a) self-consistent case and (b) self-inconsistent case.

Fig. 5 Geometric demonstration of two or zero transmitted SH waves. (a) $V \ge c_s'$; (b) $V \le -c_s'$. Because $OT^{(I)} \perp AT^{(I)}$, $T^{(I)}$ should be at a circle with diameter AO (the red dash-dotted lines, color on line). Considering that $\alpha^{(I)} \in [0, \pi/2]$, part of the circle is deleted, and the red arcs is left in the figure. By **Criterion (2)**, solid part of the red arcs means that there will be two transmitted waves if $T^{(I)}$ is at it, and dotted part of the red arcs means that there will be no transmitted wave if $T^{(I)}$ is at it.

Fig. 6 Geometric demonstration for one transmitted SH wave (BC is a chord of $\odot O_s'$. $OT^{(I)} \perp AC$). If A is at chord BC except $T^{(I)}$, the transmitted wave is evanescent.

Fig. 7 Propagation scenarios (represented as wave fronts) and the corresponding geometric demonstrations of SH waves incidence on MPI: (a) SH-i; (b) SH-ii; (c) SH-iii; (d) SH-iv; (e) SH-v; (f) SH-vi. (For interpretation of the references to color in this figure legend, the reader is referred to the web version of this article.)

Fig. 8 Propagation scenarios (represented as wave fronts) and the corresponding geometric demonstration of SV wave incidence on MPI: (a) SV-i; (b) SV-ii; (c) SV-iii; (d) SV-iv; (e) SV-v; (f) SV-vi; (g) SV-vii; (h) SV-viii; (i) SV-ix; (j) SV-x; (k) SV-xi; (l) SV-xii. (For interpretation of the references to color in the figure legend box, the reader is referred to the web version of this article.)

Fig. 9 Propagation scenarios (represented as wave fronts) and the corresponding geometric demonstration of P wave incidence on MPI: (a) P-xiii; (b) P-xiv; (c) P-v. (For interpretation of the references to color in the figure legend box, the reader is referred to the web version of this article.)

Table 1 Classification of the propagation cases of SH waves

Case (Fig. No.)	Reflected SH waves	Transmitted SH waves	Set of V	Expressions of the range of V
SH-i(Fig. 7(a))	0	0	$\mathbf{D}_{s\to s}^{(R\times 0)} \cap \mathbf{D}_{s\to s}^{(T\times 0)}$	$V = c_s \cos\alpha^{(I)}$
SH-ii(Fig. 7(b))	0	1	$\mathbf{D}_{s\to s}^{(R\times 0)} \cap \mathbf{D}_{s\to s}^{(T\times 1)}$	$c_s < \lvert V\rvert < c_s'$
SH-iii(Fig. 7(c))	0	2	$\mathbf{D}_{s\to s}^{(R\times 0)} \cap \mathbf{D}_{s\to s}^{(T\times 2)}$	$\lvert V\rvert \geq \max\{c_s, c_s'\}\ (\lvert V\rvert \neq c_s)$
SH-iv(Fig. 7(d))	1	0	$\mathbf{D}_{s\to s}^{(R\times 1)} \cap \mathbf{D}_{s\to s}^{(T\times 0)}$	$c_s' < V < c_s \cos\alpha^{(I)}$
SH-v(Fig. 7(e))	1	1	$\mathbf{D}_{s\to s}^{(R\times 1)} \cap \mathbf{D}_{s\to s}^{(T\times 1)}$	$\lvert V\rvert \leq \min\{c_s, c_s'\}\ (V \neq c_s \cos\alpha^{(I)}, c_s')$
SH-vi(Fig. 7(f))	1	2	$\mathbf{D}_{s\to s}^{(R\times 1)} \cap \mathbf{D}_{s\to s}^{(T\times 2)}$	$-c_s \leq V \leq -c_s'$ or $\max\{c_s \cos\alpha^{(I)}, c_s'\} \leq V \leq c_s$

Table 2 Classification of the propagation cases of SV wave incidence

Case (Fig. No.)	Reflected waves		Transmitted waves		Expressions of the range of V
	SV waves	P waves	SV waves	P waves	
SV-i (Fig. 8(a))	0	0	0	0	$V = \tilde{c}_s$ [1]
SV-ii (Fig. 8(b))	0	0	1	1	$c_l < \lvert V\rvert < c_s'$
SV-iii (Fig. 8(c))	0	0	2	1	$\max\{c_s', c_l\} \leq \lvert V\rvert < c_l'(\lvert V\rvert \neq c_l)$
SV-iv (Fig. 8(d))	0	0	2	2	$\lvert V\rvert \geq \max\{c_l, c_s'\}\ (\lvert V\rvert \neq c_l)$
SV-v (Fig. 8(e))	0	1	1	1	$c_s < \lvert V\rvert \leq \min\{c_l, c_s'\}\ (\lvert V\rvert \neq c_s')$
SV-vi (Fig. 8(f))	0	1	2	1	$\max\{c_s, c_s'\} \leq \lvert V\rvert \leq \min\{c_l, c_l'\}\ (\lvert V\rvert \neq c_s, c_l')$
SV-vii (Fig. 8(g))	0	1	2	2	$\max\{c_s, c_l'\} \leq \lvert V\rvert \leq c_l (V \neq \tilde{c}_s, \pm c_s)$
SV-viii (Fig. 8(h))	1	1	0	0	$c_l' < V < \tilde{c}_s$
SV-ix (Fig. 8(i))	1	1	0	1	$c_s' < V \leq \min\{\tilde{c}_s, c_l'\}\ (V \neq \tilde{c}_s)$
SV-x (Fig. 8(j))	1	1	1	1	$\lvert V\rvert \leq \min\{c_s, c_s'\}\ (V \neq \tilde{c}_s, \pm c_s')$
SV-xi (Fig. 8(k))	1	1	2	1	$-\min\{c_s, c_l'\} \leq V \leq -c_s'$ or $\max\{\tilde{c}_s, c_s'\} \leq V \leq \min\{c_s, c_l'\}\ (V \neq \tilde{c}_s, \pm c_l')$
SV-xii (Fig. 8(l))	1	1	2	2	$-c_s < V \leq -c_l'$ or $\max\{\tilde{c}_s, c_l'\} \leq V < c_s (V \neq \tilde{c}_s)$

[1] $\tilde{c}_s = c_s \cos\alpha^{(I)}$.

Table 3 Classification of the propagation cases of P wave incidence

Case (Fig. No.)	Reflected waves		Transmitted waves		Expressions of the range of V
	SV waves	P waves	SV waves	P waves	
P-i	0	0	0	0	$V = \tilde{c}_l$ [1]
P-ii	0	0	1	1	$c_l < \lvert V\rvert < c_s'$
P-iii	0	0	2	1	$\max\{c_s', c_l\} \leq \lvert V\rvert < c_l'(\lvert V\rvert \neq c_l)$
P-iv	0	0	2	2	$\lvert V\rvert \geq \max\{c_l, c_l'\}\ (\lvert V\rvert \neq c_l)$
P-v	0	1	1	1	$-\min\{c_l, c_s'\} \leq V < -c_s$ or $\max\{\tilde{c}_l, c_s\} < V \leq \min\{c_l', c_s'\}\ (\lvert V\rvert \neq c_s')$
P-vi	0	1	2	1	$-\min\{c_l, c_l'\} \leq V \leq -\max\{c_s, c_s'\}$ or $\max\{\tilde{c}_l, c_s, c_s'\} \leq V \leq \min\{c_l, c_l'\}\ (\lvert V\rvert \neq c_s, c_l')$
P-vii	0	1	2	2	$-c_l \leq V \leq -\max\{c_s, c_l'\}$ or $\max\{\tilde{c}_l, c_s, c_l'\} \leq V \leq c_l (V \neq \pm c_s, \tilde{c}_l)$
P-viii	1	1	0	0	$c_l' < V \leq \max\{\tilde{c}_l, c_s\}\ (V \neq \tilde{c}_l)$
P-ix	1	1	0	1	$c_s' < V \leq \min\{\tilde{c}_l, c_s, c_l'\}\ \ (V \neq \tilde{c}_l, c_l')$
P-x	1	1	1	1	$\lvert V\rvert \leq \min\{c_s, c_s'\}\ (V \neq \tilde{c}_l, c_s')$
P-xi	1	1	2	1	$-\min\{c_s, c_l'\} \leq V \leq -c_s'$ or $\max\{\tilde{c}_l, c_s'\} \leq V \leq \min\{c_s, c_l'\}\ (V \neq \tilde{c}_l, \pm c_l')$
P-xii	1	1	2	2	$-c_s \leq V \leq -c_l'$ or $\max\{\tilde{c}_l, c_l'\} \leq V \leq c_s (V \neq \tilde{c}_l)$
P-xiii (Fig. 9(a))	2	1	0	0	$\max\{c_s, c_l'\} < V < \tilde{c}_l$
P-xiv (Fig. 9(b))	2	1	0	1	$\max\{c_s, c_s'\} < V < \min\{\tilde{c}_l, c_l'\}$
P-xv (Fig. 9(c))	2	1	1	1	$c_s < V < \min\{\tilde{c}_l, c_s'\}$

[1] $\tilde{c}_l = c_l \cos\beta^{(I)}$.

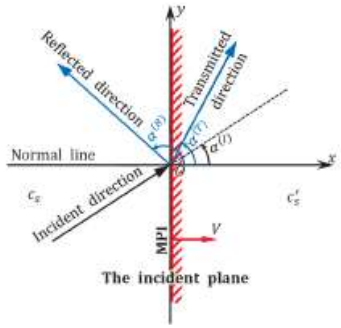

Fig 1

Fig 2

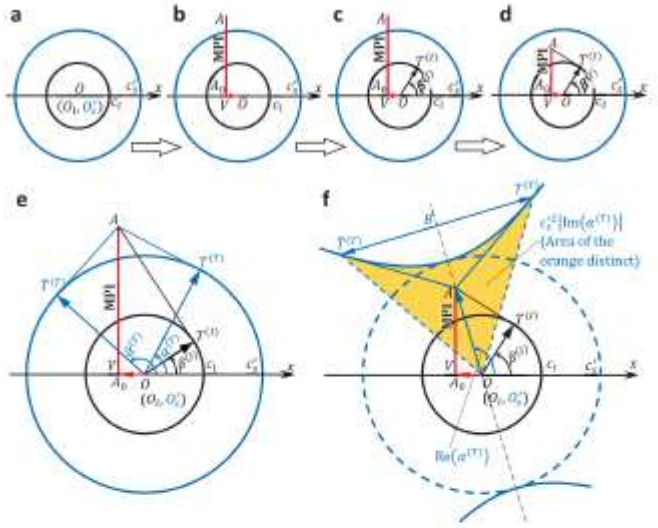

Fig 3

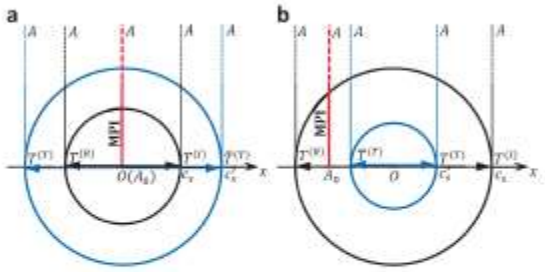

Fig 4

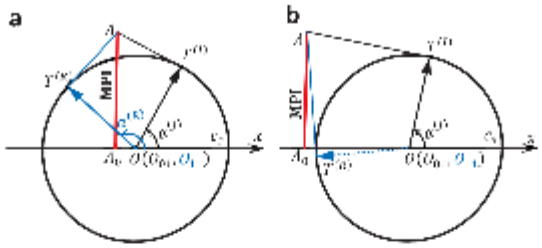

Fig 5

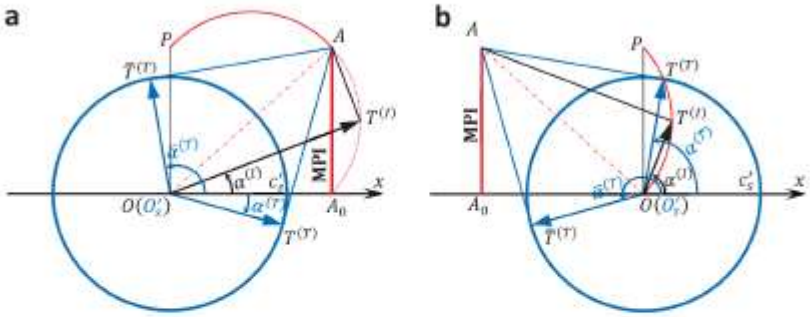
a
P
A
$T^{(T)}$
$T^{(I)}$
$\vec{R}^{(T)}$
$\alpha^{(I)}$
c_s'
MPI
x
$O(O_s')$
$\alpha^{(T)}$
A_0
$T^{(T)}$
b
A
P
$T^{(T)}$
MPI
$T^{(I)}$
$\alpha^{(T)}$
$\vec{R}^{(T)}$
$\alpha^{(I)}$
c_s'
x
A_0
$O(O_s')$
$T^{(T)}$

Fig 6

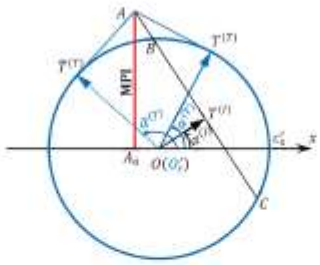

Fig 7

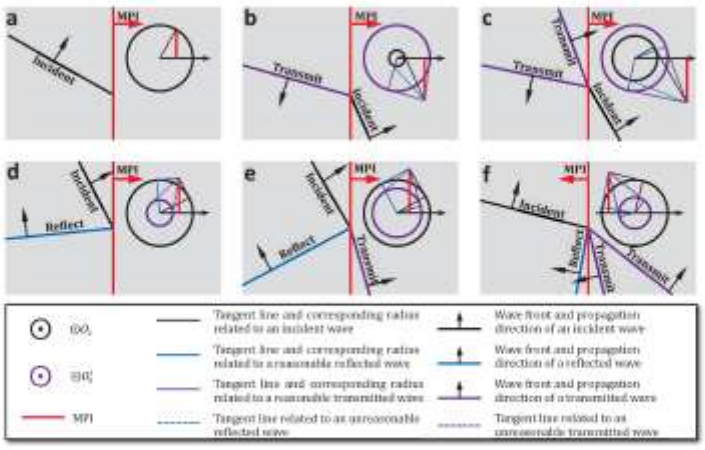

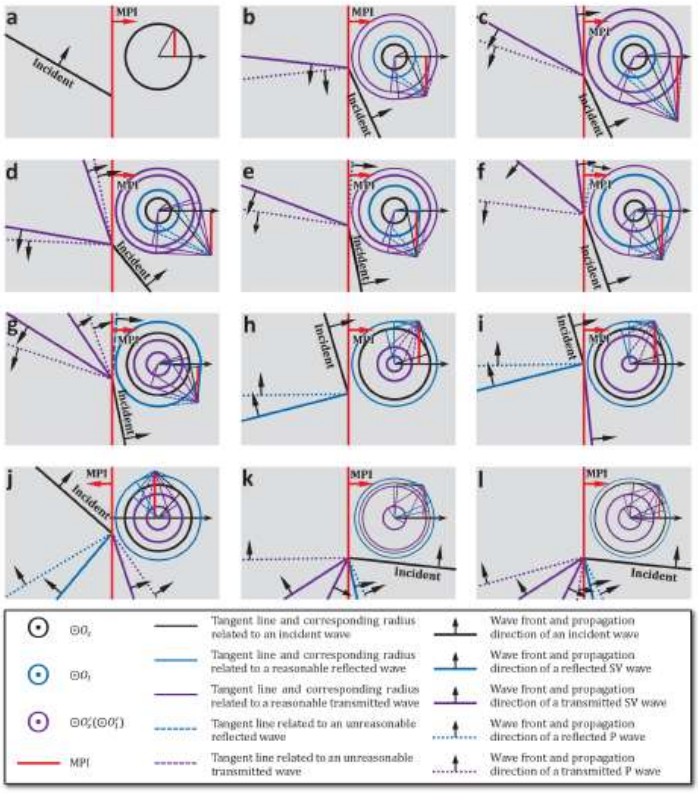

Fig 8

Fig 9

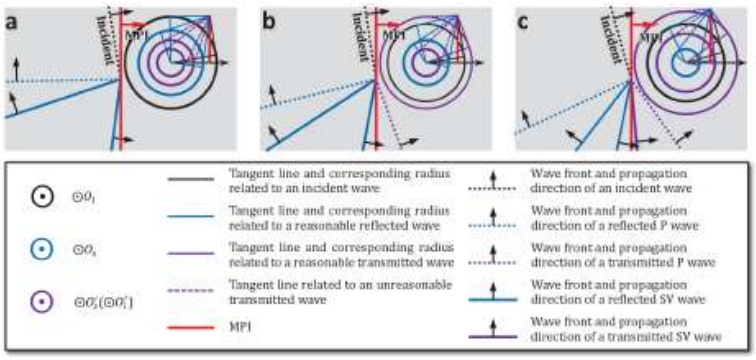
a
b
c
Incident
MPI
Tangent line and corresponding radius related to an incident wave
Tangent line and corresponding radius related to a reasonable reflected wave
Tangent line and corresponding radius related to a reasonable transmitted wave
Tangent line related to an unreasonable transmitted wave
MPI
Wave front and propagation direction of an incident wave
Wave front and propagation direction of a reflected P wave
Wave front and propagation direction of a transmitted P wave
Wave front and propagation direction of a reflected SV wave
Wave front and propagation direction of a transmitted SV wave